Lattice and charge excitations in La$_{1-x}$Sr$_x$MnO$_3$

P. Björnsson,[*] M. Rübhausen,[†] J. Bäckström, and M. Käll
Chalmers University of Technology and Göteborg University, 41296 Göteborg, Sweden

S. Eriksson and J. Eriksen
Neutron Research Laboratory Studsvik, 61182 Nyköping, Sweden

L. Börjesson
Chalmers University of Technology and Göteborg University, 41296 Göteborg, Sweden

We employ inelastic light scattering to study the dependence of the lattice and charge excitations in La$_{1-x}$Sr$_x$MnO$_3$ compounds on doping and temperature. The phonons reveal strong local lattice distortions in the paramagnetic state, which gradually vanish below the ferromagnetic transition. We identify charge excitations in the metallic state. They exhibit a dependence on the doping level and symmetry selection rules typical for a plasmonlike excitation. Their energy scale of 100 meV requires a low-carrier-density component of the plasma outlining the importance of electronic interactions in La$_{1-x}$Sr$_x$MnO$_3$.

I. INTRODUCTION

Complex phase diagrams are common to many strongly correlated systems like the cuprates, the organic superconductors, and the manganites.[1,2] In all those systems an important issue is the influence of the phononic and electronic degrees of freedom on phenomena like high-temperature superconductivity in the doped cuprates or colossal magnetoresistance (CMR) in the doped manganites.[2] Especially for the manganites it has been argued that the traditional double-exchange mechanism introduced by Zener to understand the ferromagnetic metallic state is not sufficient alone to account for the magnetic properties.[3–5] The doped compounds show many features like charge ordering and, indeed, the CMR effect itself, which are difficult to understand without taking into account the Jahn-Teller coupling between the electrons and phonons.[5–8] This view is further supported by the close relationship between the structural and electronic phase diagrams.[9,10] A detailed investigation of the electronic and lattice excitations is therefore crucial for the understanding of the manganites.

Inelastic light scattering may occur from lattice, charge, and spin degrees of freedom.[11] The crystallographic structure can be revealed in the inelastic light scattering experiments as symmetry constraints leave a footprint in the Raman-allowed phonon spectrum. The higher the crystal symmetry is, the fewer modes are Raman allowed. Iliev *et al.* and Granado *et al.* have provided a complete mode assignment for the orthorhombic LaMnO$_3$ and rhombohedral La$_{0.7}$Sr$_{0.3}$MnO$_3$.[12,13]

The coupling of light to plasmons is known from low-doped semiconductors.[14] Here, an important symmetry constraint follows from the fact that the Coulomb interaction is isotropic and, hence, plasmons occur only in configurations including the fully symmetric scattering geometry. Other properties of plasmons include a square-root-like doping dependence of the plasma frequency and a Lorentzian line shape.[15]

Raman scattering from spin excitations can occur as one- or two-magnon light scattering. The latter process is especially important for antiferromagnets.[16,19] However, in most manganites the exchange is ferromagnetic possibly with some spin canting.[17] Moreover, the antiferromagnetic end members show a layered magnetic structure with ferromagnetic exchange in the MnO$_2$ planes and antiferromagnetic exchange between them. Thus, one expects no direct magnetic scattering as long as the polarization vectors are in the MnO$_2$ planes and for frequencies investigated by Raman scattering.

In the following, we provide evidence for the strong coupling between charge, lattice, and spin degrees of freedom. We report on the presence of local Jahn-Teller-like lattice distortions in the paramagnetic state of the doped compounds, which gradually vanish around the ferromagnetic transition. For the higher-doped compounds ($x \approx 0.2$) this also leads to a metallic state, indicating the release of the charges that were coupled to the lattice. However, for smaller doping levels ($x \approx 0.1$) one still observes substantial changes in the phonon spectra of the ferromagnetic insulating state. Furthermore, we observe a plasmonlike excitation in the metallic state of La$_{1-x}$Sr$_x$MnO$_3$ due to a low-carrier-density component. These results emphasize the importance of electronic interaction effects in La$_{1-x}$Sr$_x$MnO$_3$.

II. EXPERIMENT

Polycrystalline samples have been prepared by solid-state reaction techniques using stoichiometric high-purity mixtures of La$_2$O$_3$, MnO$_2$, and SrCO$_3$. The samples have been resintered to promote crystallite growth. Typical grain sizes are 5×5 μm^2 decreasing with increasing doping level. The decreased size of the grains made polarized measurements above $x = 0.5$ impossible. Measurements have been performed in backscattering geometry on a Dilor XY800 micro-Raman setup using freshly chipped off parts of the pellets. The light was focused on typical spot sizes of about 2 μm
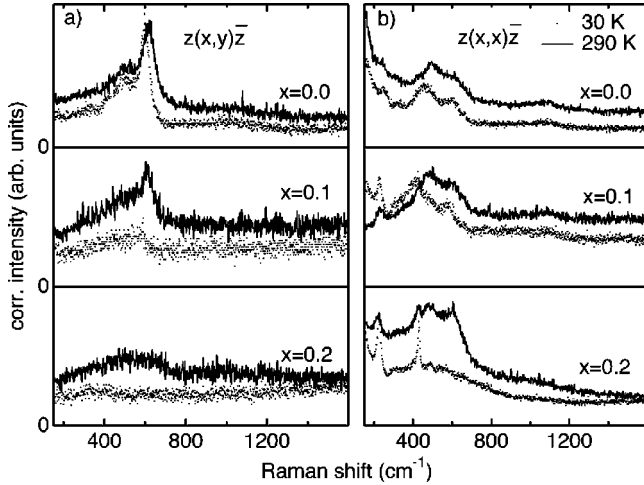
FIG. 1. Raman spectra at 290 K (solid lines) and 30 K (dots) taken with a laser excitation energy of 2.41 eV for doping levels and geometries as indicated.

using laser powers of ≤ 100 μW. The low signal as the result of the limited laser power in order to avoid structural transition effects and heating made it necessary to use compensation optics for the window of a cold-finger cryostat. All spectra displayed have been corrected for the thermal Bose factor and the spectral response of the spectrometer using a double-Ulbricht sphere system of known spectral characteristics. This corrected intensity is proportional to the Raman response after correction for the scattering volume, which can be derived from the dielectric function.[19] Measurements using different incident photon energies assure that all features are Raman signals and not due to luminescence. We use the Porto notation $z(x,x)\bar{z}$ in order to describe the polarization geometry. The first and last letters represent the directions of the incoming and the scattered photons, whereas letters in brackets indicate the incoming and scattered polarization.

III. RESULTS AND DISCUSSION

Even though there is a strong relationship between the changes of the lattice and charge degrees of freedom, we focus first on the doping- and temperature-dependent changes in the phonon spectra since they have a more straightforward discussion. Second, we outline the doping- and temperature-dependent behavior of the charge-related response in the data. Finally, we discuss the interplay between lattice and charge degrees of freedom explicitly.

A. Lattice excitations

Figure 1 shows Raman spectra of $z(x,y)\bar{z}$ geometry in (a) and $z(x,x)\bar{z}$ geometry in (b) at 290 K and 30 K for doping levels of $x=0.0$ ($T_N=155$ K), $x=0.1$ ($T_C=200$ K), and $x=0.2$ ($T_C=280$ K). At 290 K all samples are paramagnetic insulators (PIs). At 30 K they are a canted antiferromagnetic insulator (CAFI, $x=0.0$), a ferromagnetic insulator (FI, $x=0.1$), and a ferromagnetic metal (FM, $x=0.2$). The $x=0.0$ spectra are dominated by phonons around 620 and 480 cm^{-1} which are the oxygen in-phase stretching and

out-of phase bending modes of the MnO_3 octahedra. Both modes have been assigned by Iliev *et al.* and sit on a continuum.[12] In Fig. 1(a) we observe that the 620 cm^{-1} phonon softens 20 cm^{-1} below the the Néel temperature (T_N) in agreement with previous studies.[13,18,20] A comparison of $x=0.0$ and $x=0.1$ compounds shows a strong weakening of the involved modes with doping at 290 K, although the spectra are qualitatively similar. However, it is remarkable that the 620 cm^{-1} mode weakens strongly below the transition to the ferromagnetic insulating regime as indicated by the 30 K spectrum. This trend is continued in the spectra of the $x=0.2$ sample. Here, one observes at 290 K only a weak feature around the former phonon frequency and a flat continuum in the regime of the ferromagnetic metal at 30 K.

Figure 1(b) shows the phonon modes of $z(x,x)\bar{z}$ configuration. The 30 K and the 290 K spectra for the $x=0.0$ sample are essentially similar, although the 480 cm^{-1} mode softens. The additional modes at 290 cm^{-1} and 220 cm^{-1} correspond to rotations of the MnO_3 octahedra,[12] whereas the broad feature around 1100 cm^{-1} is most likely due to multiphonon scattering as indicated by its temperature dependence. For the $x=0.1$ compound the changes with temperature are more dramatic. While the 290 K spectrum shows a resemblance to the $x=0.0$ spectra at the same temperature, the 30 K spectrum shows a significant difference. First, the mode around 230 cm^{-1} becomes much more enhanced and, second, a new mode appears around 420 cm^{-1}. This observation is again supported by the $x=0.2$ compound, which shows four modes already at 290 K. Two of the phonons, i.e., the modes around 230 cm^{-1} and 420 cm^{-1}, can be attributed to phonons of the rhombohedral phase, which is the average crystallographic structure for the $x=0.2$ compound.[2,10,13] In contrast, the phonons at 480 cm^{-1} and 620 cm^{-1} are similar to the orthorhombic modes of the undoped compound. The simultaneous observation of these two sets of phonons indicates the existence of a rhombohedral structure with pronounced local orthorhombic distortions of the MnO_3 octahedra. Interestingly, the 30 K spectrum of the $x=0.2$ sample demonstrates that the orthorhombic distortions vanish at low temperatures and instead a well-ordered rhombohedral phase develops. Furthermore, it is evident that the multiphonon feature, visible as shoulder around 1000 cm^{-1}, vanishes in the 30 K spectra. Moreover, one can observe a broad hump in the 30 K spectrum centered around 460 cm^{-1}. However, no evidence of a hump can be seen in the $z(x,y)\bar{z}$ data at 30 K of the same compound indicating the A_g symmetry of this excitation. This excitation is most likely of electronic origin and discussed in detail in the next section.

To illustrate the changes of the Raman spectra for the CMR-regime compounds[2] with temperature in detail, we refer to Fig. 2 showing the $z(x,x)\bar{z}$ spectra of the $x=0.2$ compound from 370 K (paramagnetic insulator) to 30 K (ferromagnetic metal). At 370 K orthorhombic modes corresponding to those of the antiferromagnetic insulator dominate the data set, even though traces of the rhombohedral modes are visible. Cooling down to 290 K sharpens all phonons and the spectrum consists of a superposition of modes corresponding to the two competing crystallographic structures. Further cooling down to 210 K yields a strong
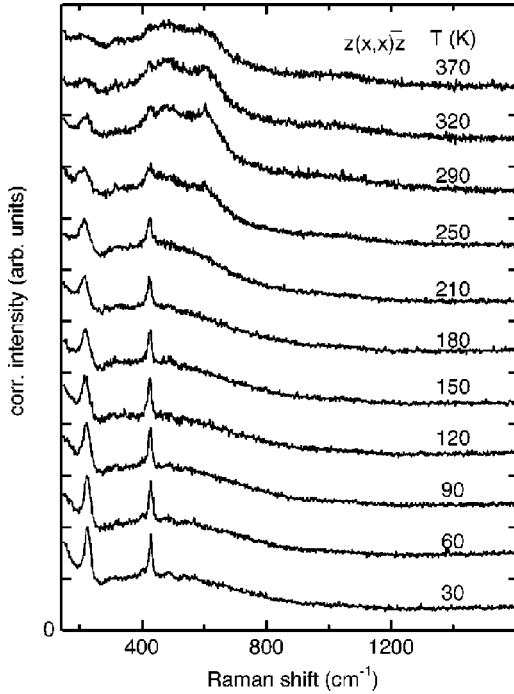
FIG. 2. Raman spectra taken with a laser excitation energy of 2.41 eV for a doping level of $x=0.2$ for temperatures between 370 K and 30 K. Base lines are indicated.

FIG. 3. Raman spectra taken with a laser excitation energy of 2.41 eV in $z(x,x)\bar{z}$ geometry at 60 K for doping levels of $x=0.2$, 0.35, and 0.5. The signal-to-noise ratio of the $x=0.5$ sample is reduced due to the decreased grain size.

increase of the scattering intensities of the modes at 420 cm^{-1} and 230 cm^{-1}, whereas the orthorhombic modes nearly vanish. We emphasize that there is no sharp change in the temperature dependence of the phonons in the investigated temperature range. Rather, we observe a continuous change of the relative intensities of phonons corresponding to rhombohedral order and orthorhombic distortions. This can be understood as a gradual change from a high-temperature rhombohedral phase influenced by strong orthorhombic distortions to a low-temperature phase with hardly any lattice distortions. As this change is strongest around the transition to the ferromagnetic metal ($T_C \approx 280$ K), it is tempting to associate the local Jahn-Teller-like lattice distortions with polarons having the tendency to localize charge carriers. Accordingly, the change in the orthorhombic distortions would imply the release of charges bound by the vanishing polarons, leading to a metallic state. The latter argumentation seems to be well in line with the results of neutron diffraction experiments.[10] However, consequently we would need to interpret similar crystallographic effects for the insulating $x=0.1$ compound as an enhancement of the carrier concentration since the strength of the orthorhombic modes decreases significantly below the ferromagnetic transition. This outlines that the carrier release for $x=0.1$ is insufficient to produce a metallic state. The latter could be a sign of additional interaction effects between the holes or the indication of a critical hole concentration needed to effectively induce percolation.

B. Charge excitations

The interpretation of the hump feature needs to be considered with care. It is clear that the hump cannot be connected to spin excitations as they should not have A_g sym-

metry and should have already appeared in the insulating antiferromangetic and ferromagnetic regimes. In Fig. 3 we follow the doping dependence of the hump at 60 K. The hump shifts in a clearly nonlinear fashion with doping towards higher frequencies from 460 cm^{-1} in the $x=0.2-740$ cm^{-1} in the $x=0.35$, and finally to 810 cm^{-1} in the $x=0.5$ compound. The increase of the hump frequency needs to be contrasted with the doping dependence of the phonons, which shift significantly towards smaller frequencies. Hence, any lattice-related origin, like a multiphonon feature, can be ruled out.
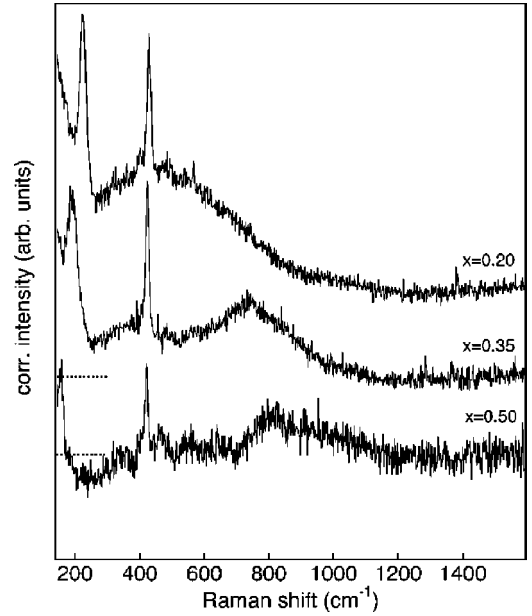
This strongly suggests an electronic origin as already indicated by the fact that the hump appears only in the metallic state. Possible scenarios for an electronic response are polarons, a collision-dominated response, or a plasmalike excitation. However, polarons can be ruled out. First, the feature shifts with increasing doping towards higher frequencies. This behavior is contrary to expectations for the polaron binding energy, which should decrease with increasing doping as the holes become more delocalized. Accordingly, Yoon et al. attributed a broad peak around 1200 cm^{-1} shifting with increasing doping towards smaller energies to a polaron.[21] Second, polarons are expected to cause local lattice distortions. However, the low-temperature phase of our metallic compounds exhibits very few distortions, making polaronic origin even less likely.

Assuming a collision-dominated response, the Raman intensity is given at $T=0$ by

$$I(\omega) \propto \frac{B_L \omega \Gamma_L}{\omega^2 + \Gamma_L^2},\qquad(1)$$

where ω denotes the frequency, B_L and Γ_L are related to the channel-dependent Raman vertex and scattering rate.[22] This equation has a peak for Raman shifts of the order of Γ_L. So
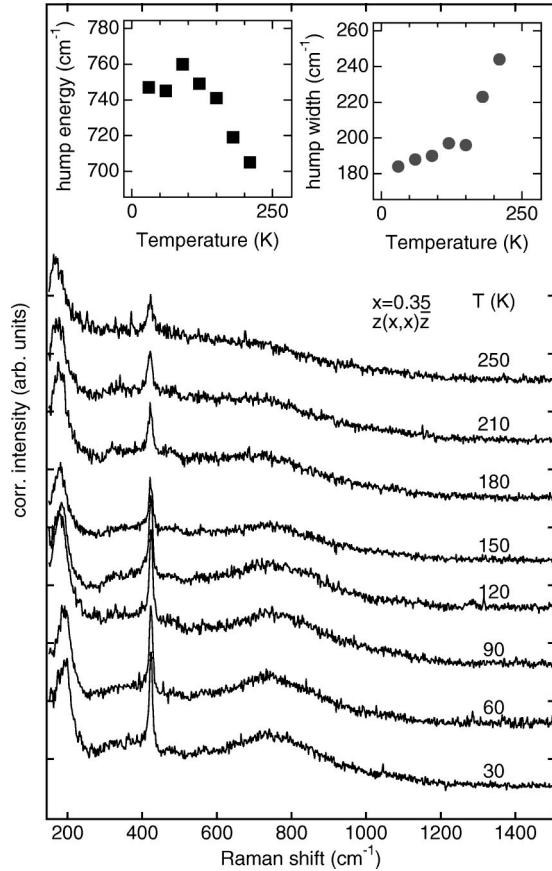
FIG. 4. Raman spectra taken with a laser excitation energy of 2.41 eV for a doping level of $x = 0.35$ displaying the temperature dependence of the hump. Temperatures and base lines are indicated. The insets give the hump energy and width derived from a fit as described in the text. Error bars are indicated by the symbol size.

assuming an extremely anisotropic scattering rate between B_{1g} ($\Gamma_{B_{1g}} \approx 5$ meV) and A_{1g} ($\Gamma_{A_{1g}} \approx 50$–$100$ meV) one might get the observed symmetry dependence shown in Fig. 1. However, unavoidably the width of the peak would increase dramatically with increasing peak frequency. This is again in clear contradiction to Fig. 3.

This leads to the remaining option that the hump is related to a collective plasmalike excitation. The symmetry selection rules follow naturally from the fact that the Coulomb interaction is isotropic. Moreover, we would expect the feature to appear only in the metallic state shifting with increasing carrier concentration towards increasing energy as clearly shown in Fig. 3. The Raman intensity of a plasmon is given as

$$I(\omega) \propto \frac{\omega_p^2 \Gamma}{(\omega^2 - \omega_p^2)^2 + \Gamma^2}, \qquad (2)$$

with $\Gamma = 2\omega_p/\tau$ and $\omega_p = \sqrt{4\pi e^2 n/m}$. Here, τ, n, and m denote the lifetime, carrier concentration, and mass of the carriers being responsible for the plasma excitation.

Figure 4 displays the temperature dependence of the hump excitation in the $x = 0.35$ compound. Since the peak frequency of the hump is for this doping level well above the energy range of the phonons, Fig. 4 allows the straightforward observation of the temperature dependence of the
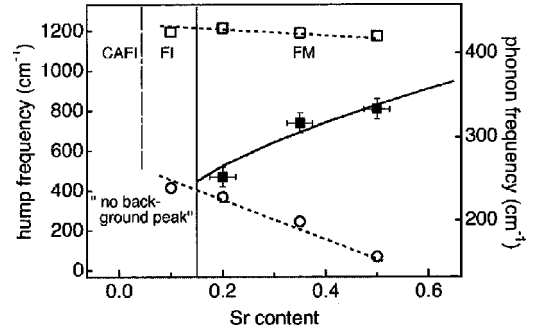
FIG. 5. Sketch of the 60 K doping dependence of the background peak (solid symbols) and phonons (open symbols). The solid line displays a square root behavior and dashed lines guide the eye.

hump. One observes a strong temperature dependence of the hump, which is dominanted by the increased thermal damping and slight peak shift towards lower energies with increasing temperatures. At roughly 250 K the hump merges with the incoherent background visible in the spectra throughout the whole temperature range. The insets display the energy and width of the hump versus temperature using a fit employing Eq. (2). The increased lifetime of the hump fits well with the expectation of a reduced electronic scattering rate at low temperatures. If we take the enhancement of the phonons as a measure that we still have a small but continued release of carriers with decreasing temperature, the observed frequency dependence appears to be in line with our expectations. Figure 4 demonstrates again that a collision-dominated response can be ruled out, as this would not yield a shift towards higher energies and a sharpening as visible in the temperature dependence of the hump.

Furthermore, if the carrier lifetime increases slightly with increasing doping, we could account for the small sharpening of the hump visible in Fig. 3. Assuming that the doping level is proportional to the Sr content we end with the plotted doping dependence of the hump as shown in Fig. 5. In fact, the doping dependence is quantitatively close to a plasmonic square-root-like behavior as indicated by the solid line and in complete contrast to the doping dependence of the phonons from which especially the 230 cm^{-1} mode seems to follow the expected soft mode behavior.[23] The key problem with our assignment is the plasma frequency expected for this doping level. It should be found, in agreement with optical spectroscopy, at frequencies of the order of 0.5–1 eV.[24] Therefore, we propose the existence of a two-component plasma with a low-carrier-density (LCD) component. The optical spectroscopies would be dominated by the high-carrier-density component, whereas Raman is much more sensitive to the LCD plasmon as screening effects, having the tendency to suppress the plasmon, become less important. An enhancement of the effective mass would not remove the discrepancy between the different spectroscopies. A two-component plasma without the existence of strong local lattice distortions directly points towards the importance of strong electronic interactions beyond the framework of a polaron-based picture.

IV. CONCLUSIONS

In conclusion, we have shown the close relationship between the spin, lattice, and charge degrees of freedom in

La$_{1-x}$Sr$_x$MnO$_3$. A gradual vanishing of the local Jahn-Teller-like lattice distortions is observed concomitant with the transition to the ferromagnetic metal in some of the doped manganites. Similar, but slightly weaker effects lead for the $x=0.1$ sample to an insulating state. This indicates that the mere existence of polaronic effects in the manganites is not sufficient for the CMR effect to occur. Furthermore, we have found a feature in the metallic phase of the manganites which we assign to a plasmon originating from a low-carrier-density component of the plasma. The latter results point towards effects emphasizing the importance of interactions between the holes doped into La$_{1-x}$Sr$_x$MnO$_3$.

*Present address: LAM Dept. of Applied Physics, Stanford University, Stanford, CA 94305-4045.

†Present address: 1006 MRL, University of Illinois, 1110 W. Green St., Urbana, IL 61801.

[1] R.H. McKenzie, Science **278**, 820 (1997).

[2] A.P. Ramirez, J. Phys.: Condens. Matter **9**, 8171 (1997).

[3] C. Zener, Phys. Rev. **82**, 403 (1951).

[4] P.W. Anderson and H. Hasegawa, Phys. Rev. **100**, 675 (1955).

[5] A.J Millis *et al.*, Phys. Rev. Lett. **77**, 175 (1996).

[6] K.H. Ahn and A.J. Millis, Phys. Rev. B **58**, 3697 (1998).

[7] I. Solovyev *et al.*, Phys. Rev. Lett. **76**, 4825 (1996).

[8] S. Ishihara *et al.*, Phys. Rev. B **56**, 686 (1997).

[9] J.F. Mitchell *et al.*, Phys. Rev. B **54**, 6172 (1996).

[10] D. Louca *et al.*, Phys. Rev. B **56**, 8475 (1997).

[11] M. Cardona, in *Light Scattering in Solids II*, edited by M. Cardona and G. Güntherodt (Springer, New York, 1982), Vol. 50.

[12] M.N. Iliev *et al.*, Phys. Rev. B **57**, 2872 (1998).

[13] E. Granado *et al.*, Phys. Rev. B **58**, 11 435 (1998).

[14] See, e.g., A. Mooradian and G.B. Wright, Phys. Rev. Lett. **16**, 999 (1966); J.F. Scott *et al.*, Phys. Rev. B **1**, 4330 (1970); M.V. Klein *et al.*, *ibid.* **6**, 2380 (1972).

[15] W. Hayes and R. Loudon, *Scattering of Light by Crystals* (Wiley, New York, 1978).

[16] P.A. Fleury and R. Loudon, Phys. Rev. **166**, 514 (1968).

[17] T.G. Perring *et al.*, Phys. Rev. Lett. **77**, 711 (1996).

[18] V.B. Podobedov *et al.*, Phys. Rev. B **58**, 43 (1998).

[19] M. Rübhausen *et al.*, Phys. Rev. B **56**, 14 797 (1997).

[20] V.B. Podobedov *et al.*, Solid State Commun. **105**, 589 (1998).

[21] S. Yoon *et al.*, Phys. Rev. B **58**, 2795 (1998).

[22] A. Zawadowski and M. Cardona, Phys. Rev. B **42**, 10 732 (1990).

[23] M.V. Abrashev *et al.*, Phys. Rev. B **59**, 4146 (1999).

[24] Y. Okimoto *et al.*, Phys. Rev. Lett. **75**, 109 (1995).